Experimental Mechanics (2015) 55:1031–1045
DOI 10.1007/s11340-015-9993-4

Non-uniqueness of the Color Adaptation Techniques in RGB Photoelasticity

D. Swain · B.P. Thomas · J. Philip · S. Annamala Pillai

Received: 18 June 2014 / Accepted: 10 February 2015 / Published online: 17 March 2015

Abstract Color adaptation in RGB photoelasticity takes care of the tint variations in a calibration specimen and the analysis image, whereby an existing calibration look-up table (LUT) is modified to adapt to the changed tint environments. The theoretical justification available for color adaptation ignores important practical aspects such as the modulation of intensities and dispersion of spectral signatures. In this paper, these nuances of color adaptation have been verified through experiments and a realistic theoretical explanation for color adaptation is provided. The experimental and theoretical analysis show that color adaptation technique produces non-unique LUTs, which is the prime reason behind the uncertainties due to color adaptation seen in the literature. This paper proposes a new strategy to overcome the non-uniqueness problem, which is validated and applied to demodulate actual fringe maps. The validation results show that the fringe maps are sufficiently smooth with 0.02 mean absolute deviation (MAD) in fringe orders. Moreover, common industrial uncertainties which can be resolved through the proposed methodology are highlighted.

Keywords RGB photoelasticity · Stress analysis · Color adaptation · Non-uniqueness problem · Theoretical calibration · Dispersion of birefringence · Modulation of intensity

D. Swain (✉) · B.P. Thomas · J. Philip
Experimental Mechanics Division, Vikram Sarabhai Space Center, Indian Space Research Organization, Trivandrum, 695 022, India
e-mail: digendranath@gmail.com

S. Annamala Pillai (Retired)
Structural Engineering Entity, Vikram Sarabhai Space Center, Indian Space Research Organization, Trivandrum, 695 022, India

Introduction

RGB photoelasticity processes a single color isochromatic image to demodulate the fringe orders. The demodulation is achieved in two steps. In the first step, a calibration look-up table (LUT) is constructed by storing the color information of the Red, Green, and Blue spectrum with respect to a linear variation of the retardation. This step is generally accomplished by conducting a bending experiment. The second step involves in comparing the colors in the analyzed image with already stored LUT by minimizing a cost function (least square error function) [2, 5, 16]. The first step is utmost important in RGB photoelasticity, since an accurate LUT would produce accurate fringe orders. Ideally, the calibration and experiments must be carried out under similar experimental conditions, e.g. illumination, camera settings, and the material of calibration [6]. This would lead to similar tint conditions in both the analysis image and the calibration image, hence RGB demodulation would be almost perfect.

The generation of LUT under the similar experimental conditions as that of a model is not always feasible, e.g. analysis of old stress frozen slices [8, 13], use of reflective photoelastic coatings during remote strain monitoring, and models prominent to ambient illumination [13]. Under these circumstances, often the actual experimental LUT is absent and/or an existing LUT is no more valid due to tint variations. The experimental factors which are responsible for tint variation are: (i) emission spectra of the illuminating source [6, 16], (ii) spectral response of the camera [6, 16], (iii) dispersion of birefringence [4, 6, 7, 14] (dependent on material and wave-length of light), (iv) transmission spectra of the material (material response, stress freezing, and aging effects) [6, 16], (v) transmission spectra of polarizing elements and camera objective [16], (vi) the quarter-wave plate

dispersion [3, 4, 6, 16], and (vii) non-uniform illumination. If a calibration LUT having different tint conditions than the analysis image is used for demodulation, it would produce erroneous fringe orders. To circumvent this issue color adaption techniques in RGB photoelasticity have been proposed by Ramesh and co-workers [11–13]. This facilitated the use of a single LUT to analyze all experimental images.

The color adaptation process generates a modified LUT interpolating the color intensities of an existing LUT to match the tints in the analyzed image. Until now one-point [11], two-point [12] and three-point [18] color adaptation schemes have been proposed. In this paper, discussions would be based mainly on two-point schemes alone, since the two-point scheme has been theoretically and experimentally shown to produce ideal LUTs to adapt to changed tint conditions [13]. In the two-point scheme, the global maxima and minima of the RGB triplet in an existing LUT are interpolated to the global maxima and minima of the individual colors available in an analyzed image. The two-point color adaptation would work well when the existing LUT and the analyzed image have 'perfect sinusoidal spectra (modulation)' for all the three colors and there is no 'dispersion of spectral signatures'. Perfect sinusoidal spectra (modulation) here implies the maxima and minima of the intensity spectrum must not vary spatially or temporally. No dispersion of spectral signature means the intensity-versus-fringe order plot of the color adapted LUT has to overlap with that of the analysis image (will be discussed in detail subsequently). In this manner, the sinusoidal behavior (modulation) of the existing LUT would be transferred to the color adapted LUT without creating any disparity in the modulations and the spectral signatures. However, images acquired through standard photoelastic experiments would always have non-uniform modulations in the intensities due to ambient and non-uniform illumination. Therefore, the analyzed image would generally have a different modulations than an arbitrary calibration specimen. Moreover, the effect of the dispersion of spectral signature would create a shift in the birefringence, which would depend upon; (i) the spectral response of the optical elements and the photoelastic material used, and (ii) the correctness of the reference LUT created during the experiments.

In the color adaptation techniques, the modulations and spectral signatures of the modified LUT might not match with those of the analyzed images. These aspects have not been considered in the available explanations of color adaptation, cf. [13]. The authors have come across significant errors after using color adaptation wherein perfectly modulated LUTs have been used for demodulating actual fringe maps [18]. This paper is thus an attempt to find out the nuances of color adaptation. Hence, initially experiments were conducted to verify the practical issues of color adaptation. Based on the experimental findings, a realistic theoretical explanation for color adaptation is provided. The analysis showed that generation of color adapted LUTs matching the behavior of analysis images are hypothetical. Therefore, only approximated LUTs can be created. If such an LUT is used for RGB demodulation, uncertainties would be introduced in the demodulated fringe orders. This would mainly depend upon the mismatch of the modulation and dispersions in the spectral behavior. Therefore, many specimen LUTs with different modulation and spectral behavior can be used for producing many color adapted LUTs. These LUTs if used for analysis, they would produce a variety of fringe orders, which makes it tough to identify the correct one.

In this paper, firstly the suitability of the color adaption schemes are investigated experimentally and theoretically. Subsequently, a theoretical RGB calibration process [18] has been proposed to mitigate this issue considering the fringe optic coefficients of the analysis material and the intensities of the analysis image. Then, the analyzed image is processed to have uniform modulation in the three color planes before analysis. The proposed method is first verified with bending calibration specimens and the fringe order uncertainties are estimated. Afterwards, the proposed work is employed to analyze samples obtained with generic and discrete fluorescent white light sources. Furthermore, the capability of the proposed method to solve practical problems are elaborated. The present work is expected to minimize the identified issues to a significant extent.

Issues with Color Adaptation Techniques

In this section, the intricacies of color adaptation technique have been verified through experimental as well as theoretical analysis. During the experimental analysis, three calibration LUTs extracted from three different specimens with varying tint conditions have been used to verify the effectiveness of color adaptation process. Subsequently, the experimental factors as reported in the introduction section are incorporated to the theoretical analysis for verifying the appropriateness of the color adaptation process.

Experimental Investigation

Three experimentally obtained LUTs from three different calibration samples have been used for analysis as shown in Fig. 1. Two LUTs have been extracted from Araldite epoxy materials with different tint conditions (different light and camera conditions). These two LUTs are named as AD-1 and AD-2 as shown in Fig. 1(a) and (b), respectively. Similarly, a third LUT has been generated from a birefringent coating made of polycarbonate (commercially available PS1 sheets, Measurements Group, US), as shown in Fig. 1(c).

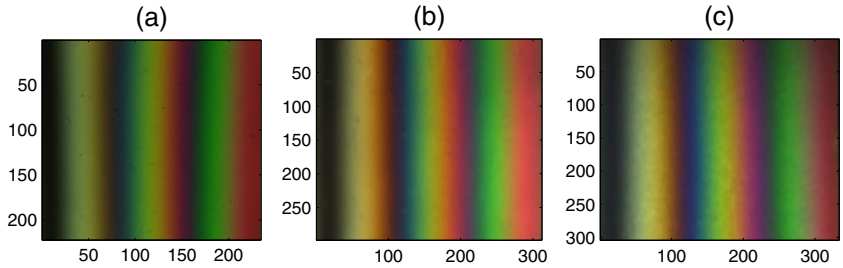

Fig. 1 The colored DF isochromatic images for three specimens obtained through bending experiments. Two specimens as shown in (**a**) and (**b**) are made of Araldite epoxy with different tint conditions. The third specimen (**c**) was made of polycarbonate (PS1) birefringent sheet. The Araldite specimens are named as AD-1, AD-2, and the polycarbonate sheet as PS

The LUT extracted from the sample AD-2 had somewhat inferior modulations in the red and green planes as evident from Fig. 3(a) and (b). Which are attributed to experimental uncertainties. Here, this specimen is intentionally considered, as a novice user from an industry would not be knowing the finer details about the LUT calibration process. Therefore, there are possibilities that such a user might employ AD-2 LUT for color adaptation and further RGB demodulation.

Initially, both Araldite LUTs have been modified using two-point color adaptation technique [12, 13] to obtain adapted polycarbonate (PS) tables. Figure 2 shows the color spectra for the LUTs obtained directly from AD-1, PS, and PS adapted from AD-1. Similarly, Fig. 3 shows the RGB spectra for AD-2, PS, and PS adapted from AD-2. The RGB spectra extracted from the three color planes in Figs. 2 and 3 show a discrepancy of the wave forms (modulations) and the occurrence of the maxima and minima of the original PS (dashed **- -** line) and adapted PS (thick solid line **–**) calibration data (dispersion of spectral signatures). The dispersion of the spectral signatures is clearly visible in the blue color planes in Figs. 2(c) and 3(c). This kind of mismatch in birefringence between different materials was earlier highlighted in Refs. [4, 6, 7]. Recently, [6] have reported issues due to dispersion in birefringence in RGB photoelasticity. The inconsistency of the modulations and the spectral

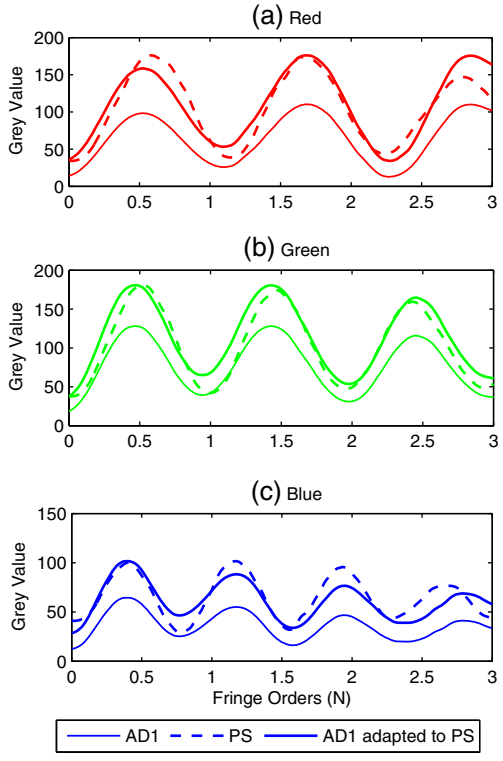

Fig. 2 The LUT data extracted for the three color planes of the specimens (**a**) red, (**b**) green, and (**c**) blue. The thin solid (–), dashed (--) and thick solid lines (**–**) correspond to the LUT of AD-1, PS , and adapted PS obtained through color adaptation of AD1, respectively

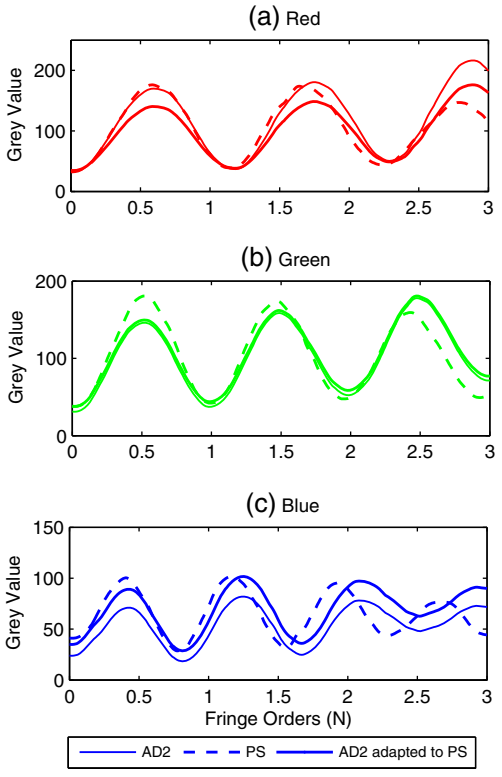

Fig. 3 The LUT data extracted for the three color planes of the specimens (**a**) red, (**b**) green, and (**c**) blue. The thin solid (–), dashed (--) and thick solid lines (**–**) correspond to the LUT of AD-2, PS , and adapted PS obtained through color adaptation of AD2, respectively

signatures are due to the experimental reasons listed in the introduction. Moreover, the behavior of the adapted PS LUTs are biased by the AD-1 and AD-2 LUTs in all the cases. It means that the color adaptation schemes attempt to scale the intensities of the existing LUT to the intensities of the analysis image without changing its spectral behavior.

The previously shown RGB spectra of the LUTs for the two color adapted cases in Figs. 2 and 3 are in two different plots, hence the comparison of the adapted PS tables and the actual PS table cannot be made. Therefore, a 3-D plot containing the RGB information for three LUTs corresponding to the adapted PS from AD1, adapted PS from AD2 and actual PS are shown in Fig. 4. The 3-D plot shows that the adapted PS tables are different than the actual one. Therefore, it can be inferred that color adaptation process does not produce a unique LUT. The effect of the non-uniqueness of the color adaptation techniques on the demodulated fringe orders is investigated next.

Herein, the effect of the mismatch in the modulation of the intensities and the spectral signatures of the color adapted LUT and the actual LUT on the RGB demodulation process has been verified. The two color adapted LUTs for PS have been used to analyze the original image of the PS specimen in Fig. 1(c). Moreover, the PS specimen is self demodulated with its own LUT. The fringe order demodulation has been carried out using the algorithm by [5] as suggested in Ref. [17]. The theoretical fringe orders are extracted from the LUT of the PS specimen, which shows an exact linear variation. The fringe orders obtained after using the two color adapted LUTs, and through self demodulation are compared with the theoretical ones.

The fringe orders obtained along a line as shown in Fig. 5(a) are plotted in Fig. 5(b). The deviation of the color adapted and the self demodulated fringe orders from the actual have been shown in Fig. 5(c). Figure 5(b) and (c) show that the fringe orders obtained through the color adapted LUTs have large deviations from the theoretical ones. The fringe orders obtained after adapting the AD-2 LUT is having more deviations as expected, since AD-2 LUT is inferior than AD-1 LUT. The fringe order deviations due to the color adapted LUTs are seen to be more towards the higher fringe orders, which are due to the spectral shifts present in the blue wavelength. This corroborates the earlier observations in Refs. [5, 6]. The self demodulated fringe orders are quiet close to the theoretical ones as expected. The above results show that the color adaptation process fetches approximate fringe orders rather than the actual ones, which also are less accurate than the self demodulated values. These kind of uncertainties due to color adaptation can be seen in the results in Refs. [11–13, 18].

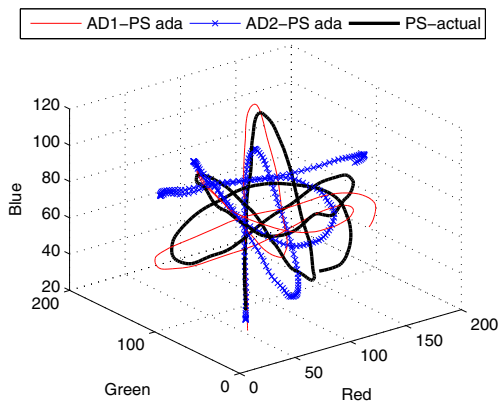

Fig. 4 The RGB curves produced using the RGB intensity information in the color adapted LUTs obtained from AD-1 and AD-2, and the actual LUT for PS are shown

The above observations can be attributed to the mismatch of the modulations and shift of spectral responses of the color adapted LUT to that of the analysis image. The ongoing discussions suggest that many LUTs can be constructed for analyzing a single image by considering different calibration samples with varying tints, which would produce differently modulated LUTs. If these LUTs are used for RGB demodulation, it would lead to some approximation of the fringe orders. If the approximation is within an acceptable band, it would be fine. However, since color adaption is used in the absence of an actual LUT for the analysis image, it is very difficult to find the deviations a-priori. These inferences imply that an LUT matching with the modulation and spectral behavior of the analysis image would be the desired one. In the next section, the observations from the experimental analysis are described theoretically. The theoretical explanation would be a realistic version of color adaptation technique which includes nuances of white light photoelasticity.

Theoretical Verification

The intensity for a certain wave-length (λ) of white light under a dark field (DF) circular polariscope arrangement neglecting the quarter wave-plate errors can be represented as [16]

$$I = I_b + \int I_0(\lambda)\gamma(\lambda)\zeta(\lambda)\sin^2[N(\lambda)\pi]\mathrm{d}\lambda, \tag{1}$$

where I, I_b and $I_0 = I_{max} - I_b$ represent the intensity at any point, the back ground and difference of the maximum and background intensities in any image, respectively. $\gamma(\lambda)$ denotes the spectral response of the camera. $\zeta(\lambda)$ is a spectral function, which includes (i) the emission spectrum of the light source, and (ii) transmission spectrum of the photoelastic material, polarizer and camera objective lens [16]. $N(\lambda)$ is the fringe order or retardation given by $N = \frac{(\sigma_1-\sigma_2)t}{f_\sigma}$, where f_σ is the fringe optic co-efficient depending on the wave-length and the material used, σ_1 and σ_2 are the

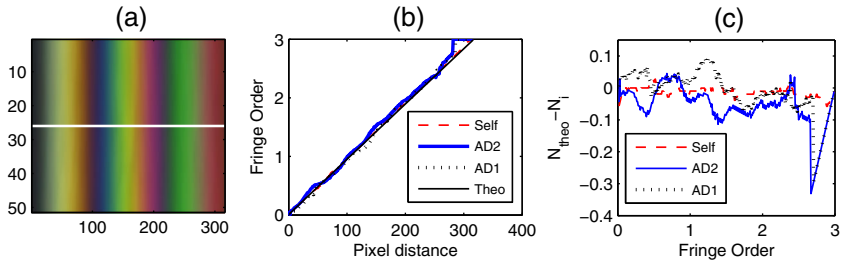

Fig. 5 (**a**) The Area of Interest (AOI) taken from the PS calibration specimen is shown along with a white line. The comparison of the fringe orders along this line using the color adapted LUTs (AD-1 and AD-2) and the actual LUT are shown in (**b**). The deviation of fringe orders obtained through color adaptation from the actual one is shown in (**c**)

principal stresses. Also, $f_\sigma = \lambda/C_\lambda$ (C_λ: stress optic coefficient). The integration has been used to represent the spread of the center wave-length known as the spectral band-width. Generally, wide bands for R, G, and B wave-lengths prevail in the generic white light illumination, other than discreet fluorescent lamps [5, 16]. Moreover, the camera RGB filters also have some band-width.

Now, the complex functions $I_0(\lambda)$, $\gamma(\lambda)$, $\zeta(\lambda)$ and $\sin^2[N(\lambda)\pi]$ are clubbed to represent as two simplified functions; (i) $s(\lambda)$ referred to as the spectral behavior and (ii) $m(\lambda)$ the modulation of the intensities. The modulation can be due to the response of various instruments and background illumination, whereas the shift in spectral signatures can enter through retardation or fringe-optic coefficients. The intensity I_0 and fringe orders N is assumed to be independent of the wave-length after using the above functions. Therefore, the above two functions can be incorporated in (equation (1)) to get the actual intensities as

$$I = I_b + \int I_0 m(\lambda) s(\lambda) \sin^2[N\pi]\mathrm{d}\lambda. \tag{2}$$

Here, it has to be noted that the maximum intensity and minimum intensity in an image are single point data, therefore they would not have any modulations. Therefore, the minimum and maximum intensities can be represented as $I_{min} = I_b$, and $I_{max} = I_b + I_0$, respectively. The analysis and calibration image with applied loads would also have the background fluctuations along with the spectral modulations. However it is difficult to separate them out. Hence, a uniform back-ground intensity has been considered for analysis. The analysis would be too complex if the above intricacies are included. Considering this, the intensities of the R, G, B color planes in the calibration LUT can be represented as

$$I_L(\lambda) = I_{bL} + \int I_{0L} s_L(\lambda) m_L(\lambda) \sin^2[N_L\pi]\mathrm{d}\lambda, \tag{3}$$

where, the maximum and minimum intensities would be $I_{maxL} = I_{bL} + I_{0L}$ and $I_{minL} = I_{bL}$, respectively, considering single point data. The subscript L used in all the symbols represents the data for an existing LUT, which would be modified for color adaptation.

Similarly, if we consider the analysis image the intensities inside the image can be represented as

$$I_A(\lambda) = I_{bA} + \int I_{0A} s_A(\lambda) m_A(\lambda) \sin^2[N_A\pi]\mathrm{d}\lambda. \tag{4}$$

Again, the maximum and minimum intensities in the analysis image would be $I_{maxA} = I_{bA} + I_{0A}$ and $I_{minA} = I_{bA}$, when considered as single point data. Here, the subscript A represents the data from the analysis image.

Now, employing the two-point color adaptation scheme [12, 13] to the LUT data and the analysis image, the intensities in the modified LUT can be found as[1]

$$I_{mod}(\lambda) = I_{bA} + \frac{I_{0A}}{I_{0L}}\left(I_{bL} + I_{0L}\int s_L(\lambda) m_L(\lambda) \sin^2[N_L\pi]\mathrm{d}\lambda - I_{bL}\right). \tag{5}$$

Equation (5) upon simplification reduces to

$$I_{mod}(\lambda) = I_{bA} + \int I_{0A} s_L(\lambda) m_L(\lambda) \sin^2[N_L\pi]\mathrm{d}\lambda. \tag{6}$$

It can be seen from (equation (6)) that the modified LUT carries the term $s_L(\lambda)m_L(\lambda)\sin^2[N_L\pi]$ of the initial LUT, which is different than $s_A(\lambda)m_A(\lambda)\sin^2[N_A\pi]$ of the analysis image as represented in (equation (4)). Hence, the theoretical investigation shows that many color adapted LUTs can be created by changing simply the modulation

[1] Two point scheme:

$$I_{mod} = I_{minA} + \frac{I_{maxA} - I_{minA}}{I_{maxL} - I_{minL}}(I_L - I_{minL}),$$

where I_{mod} are the intensities in the color adapted LUT, I_{minA} and I_{maxA} are the minimum and maximum intensities in the analysis image, I_{minL} and I_{maxL} are the minimum and maximum intensities in the existing LUT, and I_L is all the intensities in the existing LUT.

and spectral behavior of the initial LUT (considering different LUT specimen material with varying tints), which would be different than the analysis image. Therefore, it makes the color adaptation process non-unique. This non-uniqueness actually leads to uncertainties in the fringe order demodulation. At this juncture, it is very difficult to find a color adapted LUT, which would match exactly with the actual modulations and spectral behavior of the analysis image. Therefore, the color adaptation process fetches approximate fringe orders, which are not always accurate. In the next section, an alternative strategy to handle this issue would be described.

A Strategy for Overcoming the Non-uniqueness Problem

It is always difficult to determination the modulations of the intensities of the three colors in an image and construct an LUT accordingly. Moreover, the spectral behavior in the wave-lengths has to be addressed. These nuances of RGB photoelasticity has been disregarded by the color adaptation techniques proposed until now. It has been shown in the previous section that finding an ideal LUT for color adaptation is very difficult. It seems that an LUT drawn from a similar material under the same tint environment as that of the analysis sample would be the ideal one, since the spectral response and modulations would be taken care automatically. However, since experimental mode of calibration is not always feasible as discussed in the introduction, demodulation of an analysis image without any calibration specimen is attempted herein. A theoretical calibration procedure and a modified demodulation process is employed for this purpose. This procedure is expected to overcome the modulation and spectral signatures related issues.

New Calibration and Demodulation Procedure

It seems that an LUT with the actual modulation of the analysis image is the desired one, which would be a hypothetical case. From the current analysis, it can be seen that constructing a color adapted LUT matching with the behavior of a specimen is not straight forward due to many complexities. Moreover, finding the irregular modulations in an analysis image is very difficult. Hence, strategies for nullifying the effect of the modulations and the spectral behavior have been attempted.

1. The fringe optic co-efficient (f_σ) for R, G, and B wave-lengths of the analysis specimen material have to be determined. This can be an integral step for the calibration of a photoelastic material with a standard disk under compression, which is mandatory for stress calculation. Therefore, this step can be easily carried out.
2. The same camera, polariscope, and illuminating source those used for f_σ determination and grab the test image should be employed for capturing test images. However, ambient illumination can be allowed. This step also has no difficulties since light source and polariscope are often not replaced during an experiment. They are replaced after damage only. This step is suggested to avoid spectral shift. However, the experimental parameters can be changed if it doesn't disturb the spectral signature (dispersion in birefringence).
3. The intensities of light in the analysis image in all the color planes is normalized adopting the approach by [9]. Any other similar method can be used for fringe normalization, c.f. Ref. [15]. The objective of this step is to make the intensities uniformly modulated.
4. Theoretical calibration is carried out at this stage, as proposed in Ref. [18] and also described in the Appendix A employing the previously determined fringe optic coefficients, and the maximum and minimum intensities of the analysis image. This process provides a uniformly modulated LUT matching with the analysis image. Moreover, since similar f_σ values and lighting conditions are used as that of the analysis material, no shift in spectral signature is expected.
5. The above LUT is used to demodulate the normalized analysis image from step-3 by using the algorithm by [5] following the suggestions in Ref. [17].

Verification with a Calibration Specimen

The procedure detailed in the previous section is verified through a calibration specimen as it was carried out in the section "Issues with Color Adaptation Techniques". The fringe orders extracted directly from the LUT with a linear variation are again considered as the theoretical fringe orders. The same PS specimen as shown in Fig. 1(c) is used for analysis. Herein, more load was applied on this specimen to obtain fringe orders beyond four, as a result the spatial fringe order resolution per pixel decreased. Thereby, the LUT generated with this specimen can be considered worse than the specimen in Fig. 1(c), owing to the poor fringe resolution. A filament lamp is used in these experiments, therefore the modulation of the blue wavelength is expected to degrade beyond three fringe orders. Attempt to demodulate fringe orders up to four is made with such an illumination initially.

The normalized image of the PS specimen in Fig. 6(a) has been shown in Fig. 6(b). The f_σ for polycarbonate was

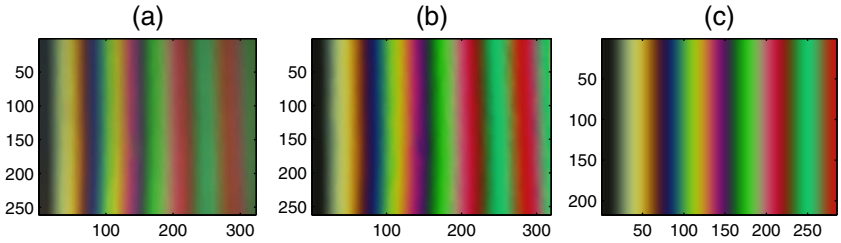

Fig. 6 (**a**) A portion of the PS calibration specimen similar to Fig. 1(c) obtained with higher load, (**b**) the normalized image of (**a**), and (**c**) the theoretically generated LUT using the f_σ values for the PS specimen are shown

determined using a disk under diametrical compression as 7.4, 6.45, 5.05 N/mm/fringe for red, green and blue wavelengths respectively using Tardy's compensation. These values along with the maximum intensity and minimum intensity of the actual specimen have been used to produce a theoretical calibration specimen as shown in Fig. 6(c). The RGB spectra for the three cases in Fig. 6 are shown in Fig. 7. Figure 7(a), (b), and (c) respectively show the spectrum of red, green, and blue colors up to four fringe orders. The R, G, B spectrum have been extracted herein with respect to green wave-length to be consistent with the theoretically generated LUT. It can be noticed in Fig. 7 that the green wave-length has four complete retardation cycles substantiating four fringe orders. The original non-uniformly modulated intensities, the modified

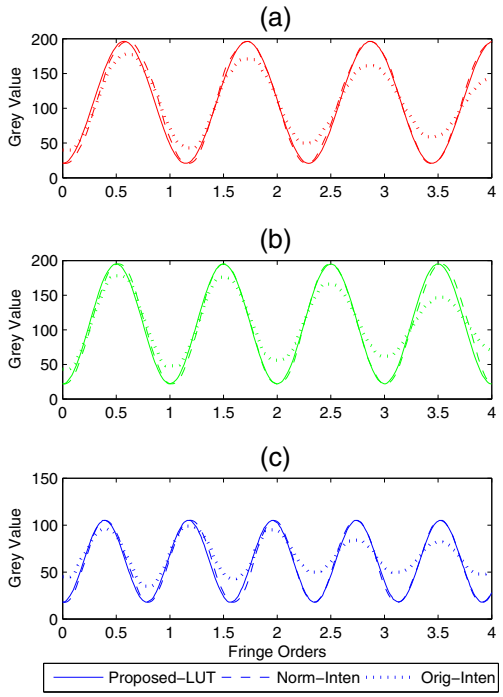

Fig. 7 The spectra for the LUT generated through the proposed work extracted from Fig. 6(c) (*solid line*), the normalized intensities of the calibration specimen extracted from Fig. 6(b) (*dashed lines*), and the intensities of the actual image extracted from Fig. 6(a) (*dotted line*) have been shown for (**a**) red, (**b**) green, and (**c**) blue color planes. The LUT contains four fringe orders

and normalized intensities, and the intensities in the theoretically proposed LUT are shown as dotted (...), dashed (- -), and solid (–) lines in Fig. 7. It also can be observed that the modulation in blue wavelength is better with the polycarbonate specimen which otherwise was absent in the epoxy specimens in AD-1 and AD-2.

Figure 7 shows that the normalized intensities and the theoretically obtained intensities are almost overlapping. Moreover, the theoretically obtained spectral signatures in all the three color planes are closer to the actual specimen. Especially, the spectral shift in the blue plane has diminished significantly. Furthermore, the normalized intensities have improved the colors in the analysis image near the higher fringe orders after intensity normalization. Also, the theoretically generated LUT is quiet smooth as compared to the experimental one. The effect of all these improvements on the demodulation process is verified next.

The isochromatic demodulation has been carried in two ways for comparison. Firstly, the specimen is self-demodulated using the LUT drawn from itself. Subsequently, the proposed demodulation procedure in this paper is implemented to obtain the fringe orders. The fringe orders obtained through self demodulation and present work are compared with the theoretical ones. The image of an area of the PS specimen containing a white line as shown in Fig. 8(a) is analyzed. The self demodulated, proposed work and theoretical fringe orders along this white line are shown in Fig. 8(b). The self demodulated fringe orders show small kinks beyond third fringe order, which is not seen in the present work. This is due to loss in modulation in blue wave-length and some amount of noise in the LUT. Kinks in fringe maps due to noisy LUTs have been reported in Ref.[17]. The theoretically obtained LUT is perfectly smooth and sinusoidal (uniformly modulated) which are difficult to obtain with a specimen if raw intensity information is used.

The demodulated fringe orders along the white line are almost overlapping for the three cases apart from the kink. Therefore, to find the relative accuracy of the proposed method, the deviation of fringe orders for the present work and self-demodulation process from the theoretical values have been estimated and shown in Fig. 8(c). It can be seen that the deviations are less than ± 0.05 fringe orders with the

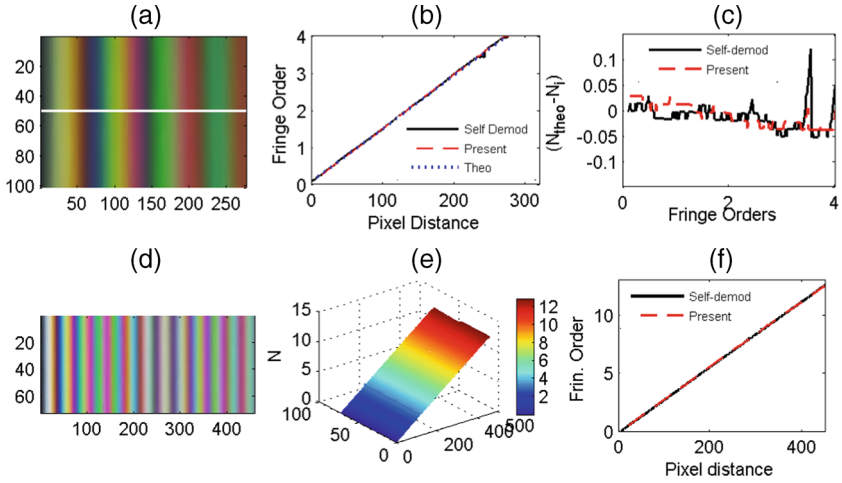

Fig. 8 The AOI of the analysis image of the previous PS calibration specimen with higher loads is shown in (**a**), the fringe orders measured along a line as shown in (**a**) through the present work, theoretical values and self-modulation are compared in (**b**) and the fringe order deviations obtained employing the proposed method and self-demodulation w.r.t the theoretical fringe orders are shown in (**c**). A DF isochromatic image of a bending specimen obtained using discrete fluorescent lamp is shown in (**d**). The demodulated fringe map for this image through the present work is shown in (**e**). Comparison of the self-demodulation and the present work are shown in (**f**). [Note: The image in (**d**) was supplied by an anonymous reviewer of the authors' paper in Ref. [18]]

present work. Thus, the results obtained using the proposed method has produced fringe orders with good accuracy, which is encouraging.

The specimen used for current verification and in the section "Issues with Color Adaptation Techniques" being the same, the fringe order deviations from the theoretical values obtained in all the cases can be compared. For a quantitative comparison of the accuracy, the mean absolute deviation (MAD), maximum and minimum absolute deviations of the fringe orders in all the cases in Figs. 5(c) and 8(c) have been estimated and reported in Table 1. The MAD is calculated by the mean of the absolute errors, which is always positive. The MAD values in Table 1 show that the self-demodulated fringe orders (case-3) are more accurate followed by the present work. It can be seen that the MAD through the color adapted processes are the large ones. Moreover, the MAD is decreased at least by 2.5 times after using the present work. The MAD obtained from the proposed work is comparable with the self-modulation values. These inferences show that the demodulation with theoretical calibration and intensity normalization can be exploited for RGB demodulation. The main requirement for the proposed method being the fringe optic coefficients alone, it can be determined easily. To this end, the proposed procedure would have an added advantage of computing stresses directly, as the fringe optic coefficients are known.

Now, the applicability of the proposed method for cases above four fringe orders is also validated. In literature, use of discrete wavelength fluorescent lamp has been advocated to expand the applicability of RGB photoelasticity to higher fringe orders (at least 12) due to the improvement in the modulation of the colors, c.f. [5, 16]. Since, discrete fluorescent lamps are not available in the authors' country, they have used images provided by an anonymous reviewer during the review of the paper in Ref. [18] as shown in Fig. 8(d). Other information about this image such as the type of material or the fringe-optic coefficients were not available.

Table 1 Comparison of the fringe order deviations estimated for the two color adapted LUTs constructed in section "Issues with Color Adaptation Techniques", two self demodulated cases considering three and four fringe orders, and the present work are reported

Sl No	Cases	Max Fringe Orders in the LUT	Mean Abs. Dev (MAD)	Min Dev	Max Dev
1	AD1-PS Col Ada	3	0.048	0.0961	0.2936
2	AD2-PS Col Ada	3	0.067	0.0452	0.3313
3	PS-self demod	3	0.015	0.0281	0.0578
4	PS-self demod	4	0.02	0.0527	0.1201
5	Present work	4	0.02	0.0387	0.0430

Therefore, to demonstrate the applicability of the proposed method the fringe optic coefficients of polycarbonate was used during demodulation. The demodulated fringe orders of Fig. 8(d) is shown in the surface plot Fig. 8(e). Figure 8(f) compares the fringe orders along a line across the image in Fig. 8(a) obtained through the present method and the self-demodulation. The demodulated fringe orders through this work are almost overlapping with the self-demodulated values. It has to be noted that this case study is a demonstration of determining higher fringe orders than the accuracy. The desired accuracy can be achieved if correct fringe optic coefficients are known.

Demodulation of Experimental Samples

Until now the verification has been carried out using LUT calibration samples through various approaches to show the functionality and accuracy of the proposed method. In this section, DF isochromatic images of three experimental samples would be demodulated as an application of the proposed method.

Two samples, (i) a disk under diametrical compression and (ii) a one-sided notch specimen made of Araldite epoxy have been considered for analysis. These samples were having f_σ values of 11.81, 10.32, and 8.38 N/mm/fringe for red, green and blue wave lengths, respectively. Similarly, a sample provided by the same anonymous reviewer using discrete fluorescent lamp is used for demodulating higher fringe orders. The sample was a C-type of hook specimen stretched with tensile loads similar to a sample shown in Ref. [5]. The properties and details of this sample was also not known as mentioned earlier.

This disk sample was not having any a-priori LUT for fringe order measurement. Therefore, an LUT from an arbitrary specimen is considered after two-point color adaptation for analysis. Similarly, a theoretical LUT as proposed in this paper is generated using the f_σ values and the intensities of the area of interest (AOI) of the analyzed disk. The color adapted LUT and the theoretical LUT are compared in Fig. 9. The LUTs were generated for four fringe orders. Figure 9 shows that the red and green wave-lengths of the color adapted LUT have not shown significant spectral shift from the theoretical ones. However, the blue wave-lengths shifts significantly after 2.5 fringe orders. Moreover, the modulations in the blue wave-length in the color adapted LUT is diminishing but not so poor. The impact of this spectral shift and non-matching modulations can be inferred from the results presented in the next paragraph.

The area of interest (AOI) chosen for the demodulation of the Araldite disk is shown in Fig. 10(a). This AOI was intensity normalized before fringe map demodulation. For demodulation using the color adapted LUT drawn from an

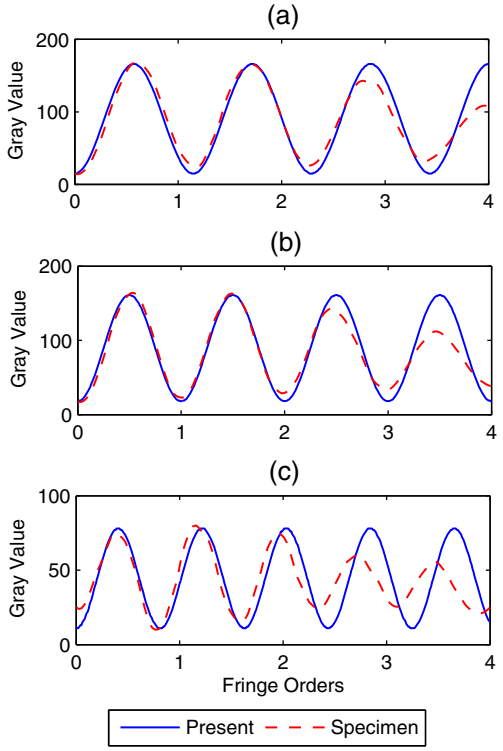

Fig. 9 The theoretical LUT as proposed in this paper (*solid line*) and a color adapted LUT extracted from an arbitrary specimen (*dashed line*) for (**a**) red, (**b**) green, and (**c**) blue wave-lengths are shown

arbitrary specimen, the original AOI is used. The demodulation is carried out up to 3.5 fringe orders. This would not be problematic as the LUTs have been created for four fringe orders. The fringe maps obtained through the proposed work and the color adapted LUT are shown in Fig. 10(b) and (c). The comparison of these two figures shows that Fig. 10(c) have big noisy areas, which is not there in Fig. 10(b). To see the quality of the fringe maps, variation of fringe order along a horizontal and a vertical lines as marked in Fig. 10(a), (b), and (c) are plotted in Fig. 10(d) and (e), respectively.

Figure 10(d) and (e) show that the fringe orders along the horizontal line show a jump after 2.8 fringe orders. This jump has influenced the whole fringe map and corrupted the smoothness. The fringe order variation along the vertical line also shows a similar jump due to the erroneous demodulation. The reasons for this erroneous demodulation beyond certain fringe orders are the spectral shifts and mismatching modulations.

The second Araldite epoxy sample as shown in Fig. 10(f) is also demodulated in a similar way as the disk. The surface plot of the demodulated fringe orders obtained for this sample are shown in Fig. 10(g). The profile of the fringe orders

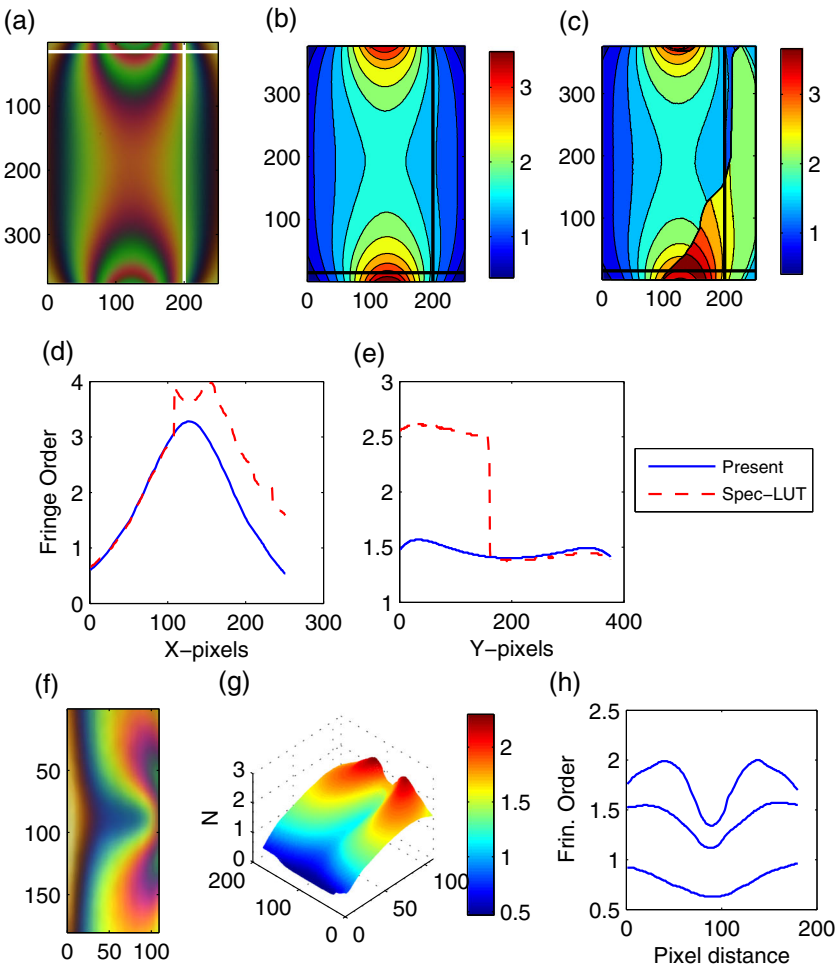

Fig. 10 The AOI of the Araldite epoxy disc used for analysis is shown in (**a**). The fringe maps demodulated using the proposed LUT and the color adapted LUT from an arbitrary specimen are shown in (**b**) and (**c**), respectively. The variation of fringe orders along (**d**) a horizontal line, and (**e**) a vertical line as shown in (**a**) are plotted. These lines are also shown in black color in (**b**) and (**c**). The AOI drawn from a one-sided notch specimen is shown in (**f**). The demodulated surface map of (**f**) is shown in (**g**) and the smoothness of the fringe orders along three vertical lines (at 10, 50, 90 pixel) of (**f**) are shown in (**h**)

along three vertical lines at 10, 50 and 90 pixels of the image in Fig. 10(f) are shown in Fig. 10(h). No comparison with other data is made for this sample as the objective was to demodulate complex fringe maps and check the smoothness of them. The profiles and the surface plot obtained are sufficiently smooth without any jumps unlike the fringe maps obtained for the disk sample. These results show that there is a good scope for the proposed work to be used as an RGB demodulation procedure, thereby the shear stresses directly. The fringe normalization works better with improved modulations, hence any improvement in the illumination would favor the proposed method.

To demonstrate the improved modulation at higher fringe orders the third sample as shown in Fig. 11(a) is used for analysis. The fringe map demodulated using the fringe optic coefficients of polycarbonate(PS) samples is shown in Fig. 11(b). The comparison of the fringe orders obtained through this work and using an LUT drawn from the sample shown in Fig. 8(d) along a horizontal line at the center of the sample is shown in Fig. 11(c). Fringe orders up to seven could be demodulated with the proposed method which is comparable to the fringe orders obtained using actual experimental LUT. Here, the accuracy and smoothness were not the objectives rather than the fringe orders. However, once correct fringe optic coefficient of this sample is known, such problems could be resolved easily.

Inferring the results presented until now, the validation and implementation of the proposed method could be completed with complex fringe maps with higher fringe orders. However, higher fringe orders could be determined using images obtained with discrete fluorescent lamps. In the next section, a generic uncertainty analysis for RGB photoelasticity would be discussed.

Solving Practical Uncertainties Through This Work

In this section, the actual experimental issues in the industries faced while using RGB photoelasticity would be deliberated. The classification of the source of uncertainties in RGB photoelasticity and the references where it is available are reported in Table 2. Some of these uncertainties are well addressed in the literature. The user has to take care of these uncertainties as per the suggestions made therein.

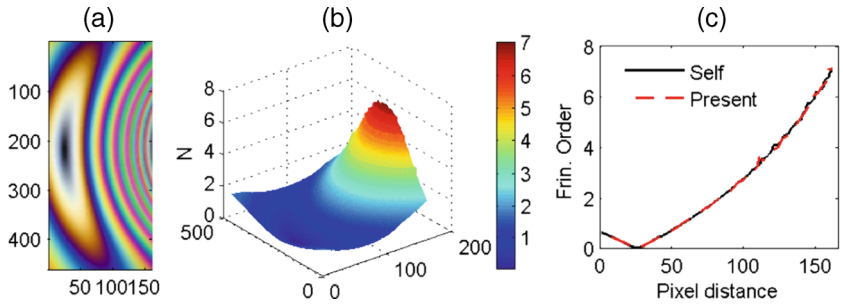

Fig. 11 A DF isochromatic image of a C-type hook sample is shown in (**a**). This image has more than six fringe orders. The demodulated surface map of the fringe orders using the properties of polycarbonate is shown in (**b**). Comparison of the fringe orders along a horizontal centerline obtained through the actual LUT (self) and the proposed work are shown in (**c**). [Note: This sample was also supplied by the anonymous reviewer as mentioned earlier]

Herein, relevant uncertainties which needs further attention have been investigated.

Effect of Intensity Modulations in a Sample

The effect of light intensity variations have been studied in Ref. [2], wherein the intensity of the whole image was decreased by using neutral filters. Such, uniform decrease in intensity have been addressed using normalized red, blue and green co-ordinates in Ref. [2]. Similarly, the effect of back-ground illumination is addressed through color adaptation in Ref. [12]. However, the light intensity variation in the same image has not been addressed.

A DF isochromatic image of a bending specimen made of Araldite epoxy with non-uniform intensities is shown in Fig. 12(a). The variation in intensities of the three colors at two different locations of the image are shown in Fig. 12(b), (c), and (d). Visually the colors in Fig. 12(a) looks similar, however there is some change in the intensities along the height of the sample. The spectral shift is almost negligible as the sample was made of the same material. The modulation along the horizontal direction is also similar. The image in Fig. 12(a) was demodulated considering LUTs drawn from the low intensity and high intensity regions. The demodulated fringe map using the high intensity LUT is shown in Fig. 12(e). Similarly, the fringe map demodulated using the low intensity LUT is shown in Fig. 12(f). Figure 12(e) shows that the regions where intensities are low are noisier, whereas the Fig. 12(f) shows that the complete fringe map is noisy. Such cases cannot be solved using color adaptation, as a single color adapted LUT cannot have two different modulations. However, this issue can be easily resolved using the proposed method. The fringe map demodulated through the present work using the fringe optic coefficients of Araldite epoxy is shown in Fig. 12(g), which is very smooth.

Effect of Tint Variation in Two Different Samples

Effect of tint variation in an LUT and an analysis image has be addressed using color adaptation [11–13, 18]. However, in this paper it has been shown that color adaptation doesn't produce the best results. To demonstrate the extreme case of RGB demodulation this case study has been carried out. A bending specimen made of Araldite epoxy with different tints have been captured as shown in Fig. 13(a) and (b). The case considered here shows that there is a change in modulation along the horizontal direction unlike the vertical

Table 2 Classification of Uncertainties in RGB Photoelasticity

Type	Name	References
Algorithmic	(1) Ambiguities	[5, 8, 10, 16, 17]
Experimental	(2) Quarter-wave plate error	[1, 2, 5]
	(3) Temporal stability	[2]
	(4) Light intensity variations	[2, 12], this work
	(5) Fringe gradient	[2], this work
	(6) Dispersion of birefringence	[6], this work
	(7) Color noise	[17]
	(8) Mis-identification of starting pixel	[5, 17]
	(9) Spectral shift due to incorrect LUT	This work
	(10) Tint variation b/w LUT and analysis image	[11–13, 18], this work

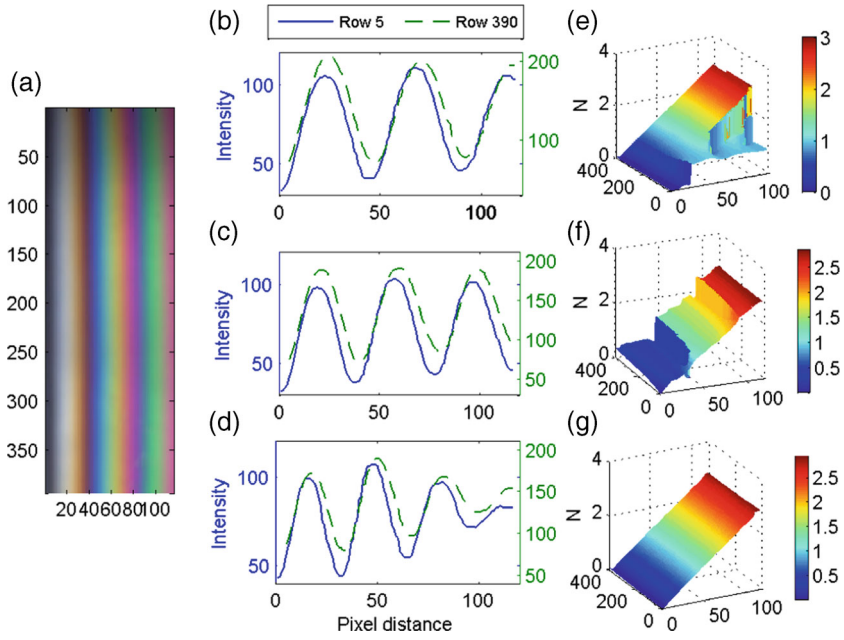

Fig. 12 A DF isochromatic image of a bending specimen with variation in intensity is shown in (**a**). The modulation of the *red, green,* and *blue* colors at two different rows are shown in (**b**), (**c**), and (**d**). The demodulated fringe maps using LUTs drawn from the high intensity (Row-390) and low intensity (row-5) zones are shown in (**e**) and (**f**), respectively. The demodulated fringe maps through the present work is shown in (**g**)

variation shown earlier. The comparison of the intensities in the three color planes for the two images are shown in Fig. 13(d), (e), and (f). It can be seen that there was almost negligible spectral shift.

The AOI drawn from Fig. 13(a) is shown in Fig. 13(c). This AOI is demodulated using the LUT drawn from Fig. 13(b). The fringe map thus obtained is shown in Fig. 13(g). This fringe map is entirely noisy as expected since there was complete mismatch of colors. The color adaptation techniques can solve this problem to a great extent but not completely. The proposed work however has solved this issue considering the fringe optic coefficients for Araldite epoxy mentioned in section "Demodulation of Experimental Samples". The fringe map obtained through the present work is shown in Fig. 13(h). The difference between the actual fringe orders and the noisy fringe orders as seen from Fig. 13(i) is very large.

Effect of Fringe Gradient and Spectral Shift

The effect of fringe gradient in RGB photoelasticity was studied in Ref. [2], wherein the image with high fringe gradient was analyzed with an LUT with low fringe gradients. However, the reverse has not been studied. Herein, a case study wherein a high fringe gradient LUT is used to demodulate a low fringe gradient image is presented. Moreover, spectral shift is introduced intentionally in the LUT. The effect of both are studied together.

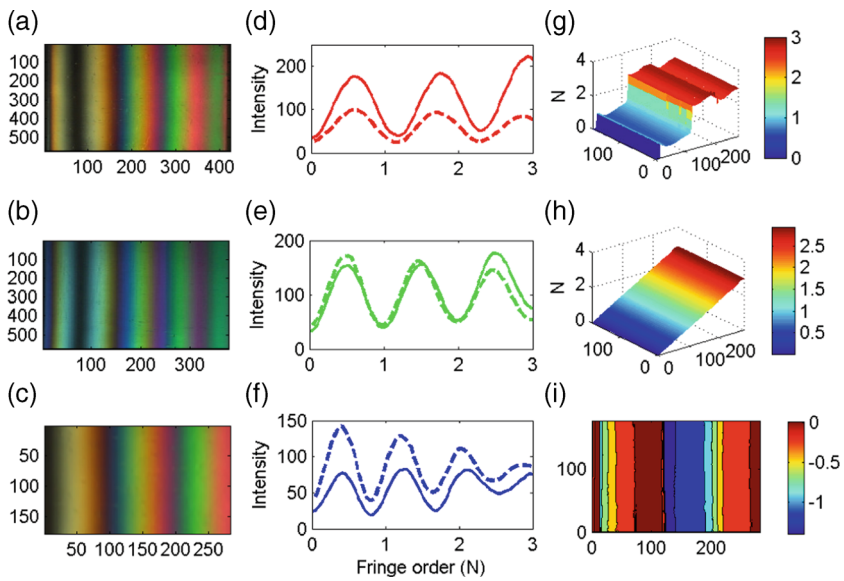

Fig. 13 The DF isochromatic image of a bending specimen with two different lighting conditions are shown in (**a**) and (**b**). The AOI of (**a**) used for analysis is shown in (**c**). The variation of the *red, green,* and *blue* color intensities along a row of the images in (**a**) and (**b**) are shown in (**d**), (**e**), and (**f**). The solid lines in (**d**), (**e**) and (**f**) are taken from (**a**). Similarly, the dotted lines are from (**b**). The demodulated fringe map of (**c**) using an LUT drawn from (**b**) are shown in (**g**). The fringe map demodulated through the present work is shown in (**h**). The difference between the actual and the noisy fringe map of (**g**) is shown in (**i**)

A synthetic bending images using the fringe optic coefficients 11.19, 10.01, and 7.997 N/mm/fringe for red, green and blue colors have been generated with different fringe gradients. The images with 0.05 and 0.005 fringes/pixel are shown in Fig. 14(a) and (b) respectively. An LUT is constructed intuitively from the image in Fig. 14(a) with a reference wavelength. Such an LUT is compared with the actual LUT drawn from Fig. 14(b) in Fig. 14(c), (d), and (e). It can be seen from these figures that there are systematic shift in the spectral signatures. The fringe orders demodulated along a row of Fig. 14(b) with the high gradient LUT are compared with the fringe orders obtained through the current work as shown in Fig. 14(f). The demodulated fringe orders through the intuitive high gradient LUT are smaller than those obtained through the present work (dashed line in Fig. 14(f)). The fringe orders through the present work seem to be smoother and accurate. Moreover, small jumps in staircase patterns can be seen in the fringe profiles obtained through the high fringe gradient LUT. Such patterns have already been reported in Ref. [17]. The fringe order difference of the proposed work (low gradient) to the high gradient LUT is shown in Fig. 14(g), which shows that the noise keeps on increasing with fringe orders. This is because the intuitive LUT had systematically induced spectral shifting.

Effect of Material Dispersion

The effect of dispersion of birefringence introduced due to different materials in RGB photoelasticity has been studied by [6]. Such case studies are also shown in section "Issues with Color Adaptation Techniques" to some extent, wherein a polycarbonate sample was demodulated using color adapted Araldite samples. Herein, the reverse would be attempted without any color adaptation.

A polycarbonate (PS) bending specimen as shown in Fig. 15(a) is demodulated using an Araldite (AD) bending specimen as shown in Fig. 15(b). The colors in both the images looks similar for visualization. The AOI of the Araldite specimen which would be demodulated is shown in Fig. 15(c). The variation of intensities of the two specimens are compared in Fig. 15(d), (e), and (f), which shows that there are large intensity variations in the red plane and some spectral shifting in the blue plane. Hence, this case is a mixture of issues due to modulation and spectral shift in different color planes. The image in Fig. 15(c) is demodulated using the PS LUT as shown in Fig. 15(g). Meanwhile, the fringe map obtained after using the present work is shown in Fig. 15(h). The RGB demdoulation through the present work is carried out considering the fringe optic coefficients of Araldite. Figure 15(g) shows a noisy fringe map while Fig. 15(h) shows a smooth fringe map. The difference between the noisy fringe map and actual one as shown in Fig. 15(i) have a large difference. The noises produced in this case corroborates well with the results in Ref. [6].

Concluding Remarks

In this paper, the nuances of color adaptation technique are discussed. It has been shown that color adapted techniques proposed until now cannot produce a unique LUT, thereby the demodulated fringe orders also. This occurs mainly due to the mismatch of the modulations of the intensities of the analysis image and the calibration LUT, and the spectral shift of the colors as a function of illumination, camera, optics and the specimen material. Therefore, strategies for eliminating the modulation and spectral shift related issues are proposed. A theoretical calibration LUT and fringe normalization procedure is used for improved

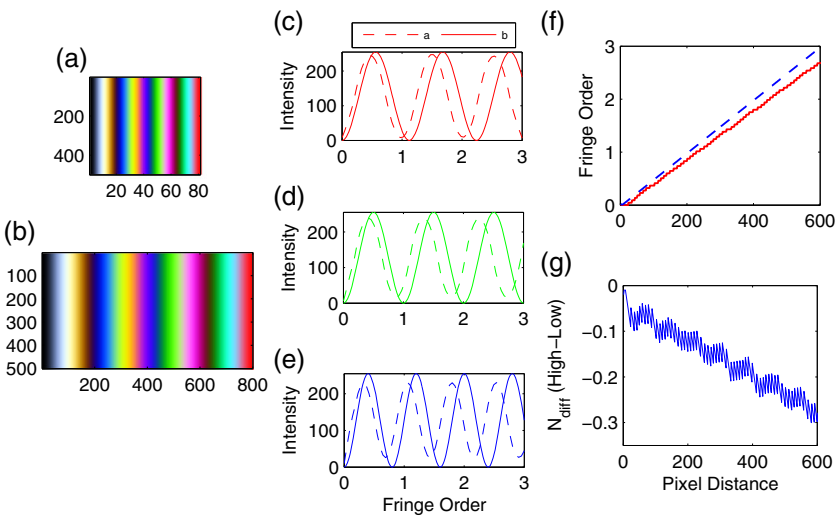

Fig. 14 Dark-field simulated isochromatic images of a bending specimen with fringe gradient of 0.05 fringes/pixel and 0.005 fringes/pixel are shown in (**a**) and (**b**). The LUTs drawn from (**a**) and (**b**) are compared in (**c**), (**d**), and (**e**). The demodulated fringe orders (*solid line* –) along a row of (**b**) using the LUT of (**a**) is compared with the present work (*dashed line* ––) in (**f**). The difference in the fringe orders due to the high fringe gradient to the low gradients are shown in (**g**)

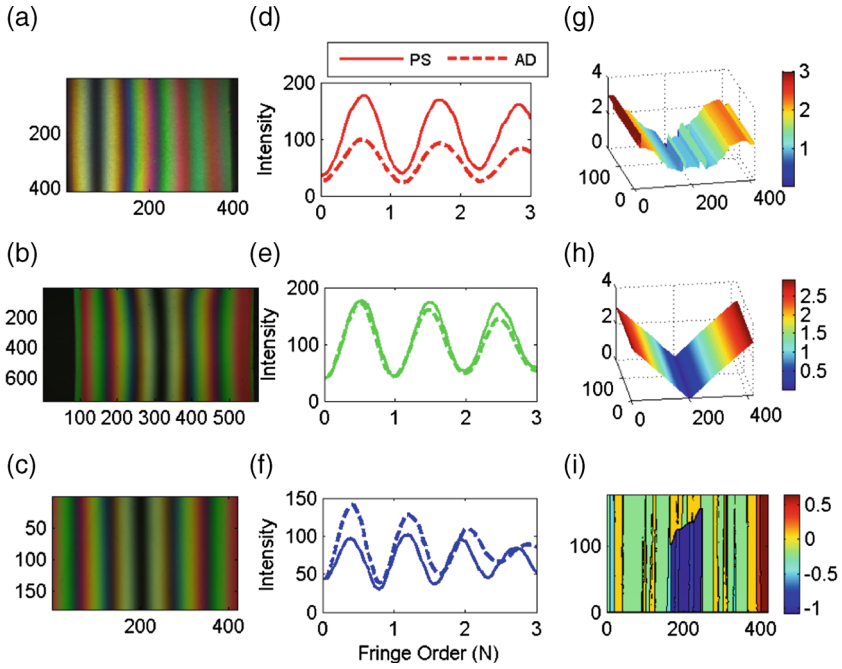

Fig. 15 The DF isochromatic image of a bending specimen made of polycarbonate (PS) is shown in (**a**). Similarly, such an image for an Araldite (AD) sample is shown in (**b**). The AOI drawn from (**b**) is shown in (**c**). The comparison of the spectral behavior of the samples in (**a**) and (**b**) are shown in (**d**), (**e**), and (**f**). The demodulated fringe map of the AOI in (**c**) analyzed using the LUT drawn from (**a**) is shown in (**g**). The fringe map demodulated through the present work up to 3 fringe orders is shown in (**h**). The difference between the actual and the noisy fringe map (**g**) are shown in (**i**)

RGB demodulation. The proposed method was validated with generic RGB calibration specimens and extended for demodulation of various experimental samples. The MAD with the proposed method is 0.02 fringe orders, and the accuracy and smoothness of the fringe orders obtained are quiet reasonable. The capability of the proposed scheme for demodulating higher fringe orders is also demonstrated using images obtained from high quality discrete fluorescent lamps. Subsequently, the uncertainties prevailing in RGB photoelasticity are classified. The relevant uncertainties which needs attention have been solved through the proposed work. Also, the proposed method can be exploited without using any experimental LUT for a specimen with the flexibility of variety of fringe gradients. Moreover, many of the uncertainties reported in the literature can be handled.

One of the issues not addressed in this work is the analysis of complex or multiply connected AOIs. Complex AOIs can be handled following the procedures in Refs. [8, 10]. The analysis of complex AOIs are just extension of the proposed algorithms with different scanning directions with many seed-points, hence are very much problem specific. Therefore, the proposed scheme is used to demodulate simple rectangular AOIs with complex fringe maps without loss of generality. The accuracy and smoothness obtained show improvement over the prevailing literature.

Acknowledgments The authors acknowledge Mr S. Karthigai Selvan (Tech Asst) and Mr S N Suresh (Technician) of EXMD, VSSC for their excellent support during experimentation. The authors also acknowledge Prof K Ramesh, Department of Applied Mechanics, IIT Madras for providing some experimental images. The authors greatly acknowledge the anonymous reviewer of their paper in Ref. [18] for providing the images captured using discrete fluorescent lamps.

Appendix A: Theoretical LUT Calibration Procedure

The procedure described below is reported in ref. [18], herein it is reproduced with minimal changes for the sake of completeness. The steps followed for creating a theoretical LUT simulating a four point bending experiment have been elaborated now. These steps can be implemented in a computer program to produce a theoretical LUT. The green-wavelength is chosen as the reference wave-length for generating the LUT. This implies that the fringe orders demodulated in an image would be w.r.t green wavelength only. The specimen chosen for the synthetic experiment is 50 mm wide and 5 mm thick.

Step 1: The maximum fringe order (N_{max}) to be generated and the fringe spatial resolution (FR) desired (fringes/pixel) needs to be specified. The width of the theoretical calibration image would depend upon the FR and N_{max}.

Step 2: The axial stress (σ_{max}) on the top and bottom fibers which are farthest from the neutral axis are estimated using the following relation

$$\sigma_{max} = \frac{(N_{max})_g (f_\sigma)_G}{t} \tag{7}$$

where, $(f_\sigma)_G$ is the fringe optic coefficient in $N/mm/fringe$ of the specimen for green wavelength as mentioned earlier. Here, the $(f_\sigma)_G$ has to

be determined for the material under study. Moreover, the (f_σ) for the red and blue wavelengths for the same materials must be determined under the same light source for use in theoretical LUT generation. Otherwise erroneous LUT would be generated.

Step 3: For generating a full-field map, the stress $\sigma(i, j)$ at each point has been calculated from σ_{max} in (equation (7)) as below

$$\sigma(i, j) = \sigma_{max}\left(\frac{|d(i, j)|}{d_{max}}\right) \tag{8}$$

Here, width is taken along the j - coordinates and length is taken along i - coordinates (axial direction). For a whole field picture, 500 pixels are considered along length direction to simulate some portion of a bending specimen, $d_{max} = w/2$ is 25 mm and $d(i, j)$ varies from zero to $\pm d_{max}$ in mm. Also, $-d_{max} < d(i, j) < d_{max}$. The zero value corresponds to the neutral axis.

Step 4: Full-field fringe orders are determined for all the color planes as given below

$$\begin{aligned} N_R(i, j) &= \frac{\sigma(i,j)t}{(f_\sigma)_R} \\ N_G(i, j) &= \frac{\sigma(i,j)t}{(f_\sigma)_G} \\ N_B(i, j) &= \frac{\sigma(i,j)t}{(f_\sigma)_B} \end{aligned} \tag{9}$$

where, N_R, N_G and N_B are the fringe maps for red, green and blue colors and $(f_\sigma)_R$, $(f_\sigma)_G$ and $(f_\sigma)_B$ are the corresponding fringe optic coefficients, which have been determined previously.

Step 5: Now the intensities of individual wavelengths has been estimated using the whole-field fringe maps for respective colors obtained in (equation (9)) for DF isochromatic conditions using the following expression

$$I_k(i, j) = I_{kb} + I_{k_0}\left(\sin\left[N_k(i, j)\pi\right]\right)^2 \tag{10}$$

where, I_k is the whole-field intensity for individual wavelengths, I_{k_0} is the difference in the maximum and back ground intensities for the respective wavelengths, and $k = R, G, B$. Here I_{bK} is the background intensity. The back ground intensity and the maximum intensities have to be determined from the analysis image after fringe normalization.

Step 6: Now, since the exact location of the neutral axis and the maximum fringe order in pixel dimensions are known, there would not be any ambiguity in selecting the corresponding pixels. The horizontal center pixel and the end pixel in the calibration image correspond to the neutral axis and the maximum fringe order, respectively. Therefore an indexed LUT can be created accurately and stored for further use.

References

1. Ajovalasit A, Barone S, Petrucci G (1995) Automated photoelasticity in white light: influence of quarter-wave plates. J Strain Anal 30(1):29–34
2. Ajovalasit A, Barone S, Petrucci G (1995) Towards RGB photoelasticity: full field automated photoelasticity in white light. Exp Mech 35(3):193–200
3. Ajovalasit A, Barone S, Petrucci G, Zuccarello B (2002) The influence of the quarter wave plates in automated photoelasticity. Opt Lasers Eng 38(1–2):31–56
4. Ajovalasit A, Petrucci G, Scafidi M (2007) Phase shifting photoelasticity in white light. Opt Lasers Eng 45(5):596–611
5. Ajovalasit A, Petrucci G, Scafidi M (2010) RGB photoelasticity: review and improvements. Strain 46(2):137–147
6. Ajovalasit A, Petrucci G, Scafidi M (2012) RGB photoelasticity applied to the analysis of membrane residual stress in glass. Meas Sci Technol 23(2):025,601 (1–8)
7. Haake SJ, Patterson EA (1993) The dispersion of birefringence in photoelastic materials. Strain 29(1):3–7
8. Kale S, Ramesh K (2013) Advancing front scanning approach for three-fringe photoelasticity. Opt Lasers Eng 51:592–599
9. Larkin KG, Bone DJ, Oldfield MA (2001) Natural demodulation of two-dimensional fringe patterns. I. general background of the spiral phase quadrature transform. J Opt Soc Am A 18(8):1862–1870
10. Madhu KR, Ramesh K (2007) Noise removal in three-fringe photoelasticity by adaptive color difference estimation. Opt Lasers Eng 45(1):175–182
11. Madhu KR, Prasath RGR, Ramesh K (2007) Color adaptation in three fringe photoelasticity. Exp Mech 47(2):271–276
12. Neethi SB, Ramesh K (2011) Color adaptation in three fringe photoelasticity using a single image. Exp Tech 35(5):59–65
13. Neethi Simon B, Kasimiyan T, Ramesh K (2011) The influence of ambient illumination on color adaptation in three fringe photoelasticity. Opt Lasers Eng 49(2):258–264
14. Pindera JT, Cloud G (1966) On dispersion of birefringence of photoelastic materials. Exp Mech 6(9):470–480
15. Quiroga JA, Servin M (2003) Isotropic n-dimensional fringe pattern normalization. Opt Commun 224:221–227
16. Quiroga JA, García-Bottela A, Gómez-Pedrero JA (2002) Improved method for isochormatic demodulation by RGB calibration. Appl Opt 41(17):3461–3468
17. Swain D, Philip J, Pillai SA (2014) A modified regularized scheme for isochromatic demodulation in RGB photoelasticity. Opt Lasers Eng 61:39–51
18. Swain D, Thomas BP, Philip J, Pillai SA (2015) Novel calibration and color adaptation schemes in three-fringe RGB photoelasticity. Opt Lasers Eng 66:320–329